PCCP

# Mechanism and Kinetics for the Reaction of Methyl Peroxy Radical with O2


| | |
|---|---|
| Journal: | *Physical Chemistry Chemical Physics* |
| Manuscript ID | CP-ART-06-2021-002427.R1 |
| Article Type: | Paper |
| Date Submitted by the Author: | 31-Aug-2021 |


| | |
|---|---|
| Complete List of Authors: | Lakshmanan, Sandhiya; CSIR-National Institute of Science, Technology and Development Studies,<br>Hase, William; Texas Tech University, Depart of Chemistry and Biochemistry<br>Smith, Gregory; SRI International |

# Mechanism and Kinetics for the Reaction of Methyl Peroxy Radical with $O_2$

Sandhiya Lakshmanan,[a,b*] William L. Hase[a,c],Gregory P. Smith[d*]

[a]Department of Chemistry and Biochemistry
Texas Tech University
Lubbock, Texas 79409 USA

[b]CSIR - National Institute of Science, Technology and Development Studies
New Delhi-110060
India

[c] deceased

[d] SRI International
Menlo Park CA 94025 USA

*Corresponding authors E-mail: sandhiya@nistads.res.in
gregory.smith@sri.com

**Abstract**

Quantum chemical calculations and dynamics simulations were performed to study the reaction between methyl peroxy radical ($CH_3O_2$) and $O_2$. The reaction proceeds through three different pathways (1) H-atom abstraction, (2) $O_2$ addition and (3) concerted H-atom shift and $O_2$ addition reactions. The concerted H-atom shift and $O_2$ addition pathway is the most favourable reaction both kinetically and thermodynamically. The major product channel formed from these reactions is $H_2CO + OH + O_2$. Trajectory calculations also confirm that $H_2CO + OH + O_2$ is the main product channel. An estimated rate constant expression for this reaction from master equation calculations is $4.20x10^{13}e^{-8676/T}$ $cm^3mole^{-1}s^{-1}$.

## I. Introduction

Combustion and ignition of natural gas, of which methane is the main component, is somewhat slower than other fuels mainly due to the relatively slow reactivity of the dominant early methyl radical.[1] A wide range of conditions are encountered, which need reliable kinetic modelling. Recent interests including engines, turbines, rockets, and oxy-fuel combustors extend this range to very high pressures and oxygen concentrations. Thus from a mechanism point of view it is important to examine sequential methyl reactions with oxygen. Under certain conditions, significant partial equilibrium concentrations of relatively unreactive methyl peroxy radical, $CH_3O_2$ can be present. Thus it is appropriate to ask, for high oxygen environments, whether this radical could react with oxygen, as even a slow rate constant could be significant. No such reactions are in current combustion mechanisms or kinetics databases.

The oxidation of $CH_3$ by molecular oxygen ($^3O_2$) is one of the most important reactions in combustion processes and the reaction plays a key role in methane ignition. The reaction takes place via four reaction channels as shown below:

$$CH_3 + O_2 \rightarrow CH_3O_2 \qquad (R1)$$

$$CH_3 + O_2 \rightarrow CH_2O + OH \qquad (R2)$$

$$CH_3 + O_2 \rightarrow CH_3O + O \qquad (R3)$$

$$CH_3 + O_2 \rightarrow HCO + H_2O \qquad (R4)$$

The formation of methyl peroxy radical R1 ($CH_3O_2$) is pressure dependent and dominates at temperatures below 1000 K.[2-4] This association process is exothermic by 29.5 kcal/mol calculated at G2 (QCISD(T)/6-311+G(3df,2p) level of theory.[4] The reactions R2 and R3 are chain branching and important and competitive at higher temperatures.[1] R2 initially forms $CH_3O_2$ radical which further undergoes H-atom shift/OH elimination reactions leading to the final products.[5] The products of R3 are formed via $CH_3O_2$ by fragmentation reaction. Reaction R4 is highly exothermic but it is a kinetically non-competitive reaction.[5,6] A very earlier RRKM calculation reported that the formation of $CH_3O_2$ (R1) dominates the $CH_3 + O_2$ process upto ~ 1500 K, before the reactions R2 and R3 become competitive.[7] This reveals that up to 1500 K, $CH_3O_2$ is amply present in the combustion system and plays an important role in methane oxidation chemistry under high-pressure intermediate-temperature conditions.[8]

Under combustion conditions at temperatures of 500-600 K, sequential addition of $O_2$ molecules to hydrocarbon/oxygenated radicals leads to highly oxygenated molecules.[9] The peroxy radicals generate cool flames at these temperatures, and ignition exhibits a negative temperature coefficient behaviour leading to engine knock.[10,11] In new high pressure turbine uses of methane, due to high oxygen density and low temperature ignition, $CH_3O_2$ could be more prone to react with molecular oxygen ($^3O_2$). The reaction is expected to lead to the following product channels which are extremely exothermic:

| | $\Delta H_{298}$ [kcal/mol] | |
|---|---|---|
| $CH_3O_2 + {}^3O_2 \rightarrow CO + H_2O + HO_2$ | -84.3 | (R5) |
| $CH_3O_2 + {}^3O_2 \rightarrow CO_2 + H_2 + HO_2$ | -94.1 | (R6) |
| $CH_3O_2 + {}^3O_2 \rightarrow HCOOH + HO_2$ | -90.5 | (R7) |
| $CH_3O_2 + {}^3O_2 \rightarrow CO_2 + H_2O + OH$ | -145.9 | (R8) |

The reaction enthalpies given are calculated from the enthalpies of formation of the reactive species available in Active Thermochemical Tables (ATcT).[12] However, to date none of these reactions has been considered in combustion mechanisms, nor have measurements or computations been reported. It is particularly important to examine these possibilities for applications at high pressures or oxy-combustion conditions where ignition and $CH_3O_2$ intermediates are important.

Given the potential importance of peroxy radicals for ignition in high pressure and oxy-combustion systems, it is vital to determine the formation of chain carriers and the mechanism for reaction products of R5-R8. The present study explores in detail all the possible reaction pathways for the reaction between $CH_3O_2$ and $^3O_2$ using quantum chemical methods. The reaction mechanism is established with specific emphasis on predicting the key elementary steps and the lowest energy pathway for the $CH_3O_2 + {}^3O_2$ reaction, which may serve as a prototype for sequential addition of $O_2$ to peroxy radicals. The key reactions involved in this combustion system are identified and the kinetics of the reactions are calculated. The results will have greatest importance for methane oxidation and ignition under high pressure, high oxygen, and supercritical conditions, for example in methane fuelled engines, turbines, and rockets.

## II. Computational Methodology

The structures of all the stationary points on the ground state potential energy surface (PES) of $CH_3O_2 + O_2$ reaction system are optimized at DFT-M06-2X functional[13] with cc-

pVTZ basis set.[14] The M06-2X method has been benchmarked and recommended for main group elements for determining thermochemistry and kinetics.[13] Vibrational frequencies of the stationary points (intermediates and transition states) were calculated at the same level of theory and minima were confirmed, with all positive frequencies and transition states having one imaginary frequency. The optimization of stationary points and frequency calculations were performed with tight convergence criteria and an ultrafine integration grid. Intrinsic reaction coordinate (IRC) analysis was performed to check the connectivity of the reactants and the corresponding products. For very few reactions, the IRC calculations failed due to the low curvature of the PES and hence, for these reactions potential energy surface scans were performed to understand the behaviour of the transition states. Single point calculations at CCSD(T)/cc-pVTZ level[15,16] on the structures obtained at M06-2X/cc-pVTZ level of theory were performed to check the reliability of the M06-2X functional for this reaction. Wherever necessary, an unrestricted ansatz was used and the stability of the wave function was checked to ensure that low-spin open shell solutions were found to the Kohn-Sham equations. All the calculations were performed on a doublet PES. To benchmark the CCSD(T)/cc-pVTZ and M06-2X/cc-pVTZ levels for the current reaction, thermochemistry of selected reactions were also calculated at CBS-QB3 method,[17] which has been evaluated as the most accurate method for reactions involving oxygen-centered radicals.[18,19] All the electronic structure calculations were performed with Gaussian 09 program.[20]

Post-transition state dynamics simulations were performed with the VENUS chemical dynamics computer program[21,22] interfaced with the NWChem electronic structure program.[23] The simulations were initiated from the transition states, such that transition state theory (TST) is valid for the reactions studied. The vibrational and rotational energies for the transition states were sampled from their Boltzmann distributions for a temperature of 300 K. These energies were transformed into the Cartesian coordinates and momenta required for trajectory calculations using quasiclassical sampling.[24] The vibrational modes at TS are excited using quasiclassical sampling, which includes zero-point energy (ZPE). A sixth-order symplectic algorithm was used to integrate the trajectories numerically.[25,26] The total integration time for each trajectory was 2 ps. Selection of initial conditions for the trajectories are standard options in VENUS.[21,22] This simulation procedure was used in our earlier studies for post-transition state dynamics simulations.[27,28] Rate constant expressions were then computed using transition state theory and master equation calculation results based on the potential energy surface energy and vibrational mode data from the quantum calculations. Codes from the Multiwell package were used.[29]

## III. Results and Discussion

### A. Mechanism and Reaction Pathways:

Reaction enthalpies for reactions R5-R8 calculated at various levels of theory and compared with the ATcT data[12] are presented in Table 1. The composite method CBS-QB3 gives thermochemical data in closer agreement with the ATcT values. The enthalpy calculated at UCCSD(T)/cc-pVTZ level with thermochemical corrections from UM06-2X/cc-pVTZ level is closely matched with CBS-QB3 values. The UM06-2X/cc-pVTZ level predict enthalpies with lower values than the CBS-QB3 and coupled cluster methods. Considering the good agreement results for thermochemistry calculations at the UCCSD(T)/cc-pVTZ level with thermal corrections from the UM06-2X/cc-pVTZ level, the results obtained for the potential energy surface at the UCCSD(T)/cc-pVTZ level are discussed in the manuscript.

**Table 1:** Enthalpy ($\Delta H_{298}$, kcal/mol) of reactions R5-R8

| Reactions | CBS-QB3 | M06-2X/cc-pVTZ | UCCSD(T)/cc-pVTZ | ATcT[12] |
|---|---|---|---|---|
| $CH_3O_2 + {}^3O_2 \rightarrow CO + H_2O + HO_2$ | -83.9 | -77.9 | -82.2 | -84.3 |
| $CH_3O_2 + {}^3O_2 \rightarrow CO_2 + H_2 + HO_2$ | -95.7 | -91.2 | -92.7 | -94.1 |
| $CH_3O_2 + {}^3O_2 \rightarrow HCOOH + HO_2$ | -90.7 | -88.5 | -88.3 | -90.5 |
| $CH_3O_2 + {}^3O_2 \rightarrow CO_2 + H_2O + OH$ | -145.9 | -139.7 | -142.9 | -145.9 |

The reaction between $CH_3O_2$ and $^3O_2$ proceeds via three different initial steps: (1) H-atom abstraction, (2) $O_2$-addition and (3) a concerted $O_2$ addition and H-shift reaction, as shown in Scheme 1.

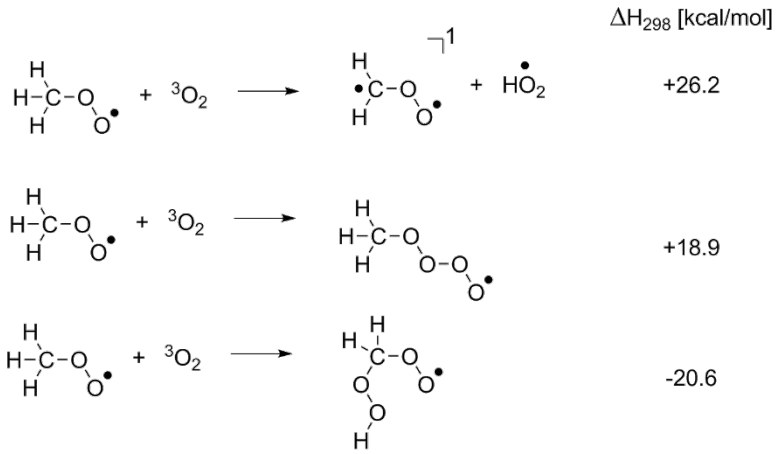


**Scheme 1.** Initial steps involved in the reaction between $CH_3O_2$ and $^3O_2$. The enthalpy values calculated at UCCSD(T)/cc-pVTZ level are given.

As can be readily seen from the thermochemistry illustrated in Scheme 1, the concerted $O_2$ addition and H-shift reaction results in an adduct that is the thermodynamically favourable initial step in the reaction between $CH_3O_2$ and $^3O_2$. The H-atom abstraction forming $CH_2OO$ and $HO_2$ is a much less feasible reaction thermodynamically. The mechanistic and kinetic aspects of these initial reactions and further secondary reactions are discussed in the following sections.

**H-atom abstraction reaction:**

The PES for H-atom abstraction reaction is shown in Figure 1, where the energies are given with vibrational zero-point corrections, $\Delta H_0(0)$. The reaction between $CH_3O_2$ and $^3O_2$ initially forms a pre-reactive complex (RC1a) with a very low stability of 0.7 kcal/mol. The $^3O_2$ abstracts a H-atom from $CH_3O_2$ forming $CH_2OO$ + $HO_2$ through a loose transition state TS1a with energy barrier of 42.6 kcal/mol. One expects most trajectories from this transition state to form the abstraction products directly. This is the lowest energy path following TS1a, with 16.5 kcal/mol enthalpy released.

A product channel complex exists between $CH_2OO$ and $HO_2$, PC1a, at 16.5 kcal/mol above the isolated reactants and requires 11.9 kcal/mol to break into the products $CH_2OO$ and $HO_2$. An extensive reorientation along the surface is required to reach this configuration. In the presence of $HO_2$, $CH_2OO$ in this complex further undergoes isomerization to a dioxirane complex with $HO_2$ with an energy barrier of 34.4 kcal/mol through TS2a. The product complex of dioxirane and $HO_2$ (PC2a) lies 5.8 kcal/mol below the isolated reactants. PC2a further isomerizes to methylenebis(oxy) isomer, PC3a by O-O bond cleavage through TS3a with energy barrier of 11.4 kcal/mol. PC3a lies just 1 kcal/mol below the TS3a and further undergoes unimolecular dissociation to several products. The methylenebis(oxy) isomer in PC3a results in the formation of formic acid, PC4a through an H-atom shift reaction passing via TS4a with an activation energy of 2.4 kcal/mol with respect to the separated reactants.

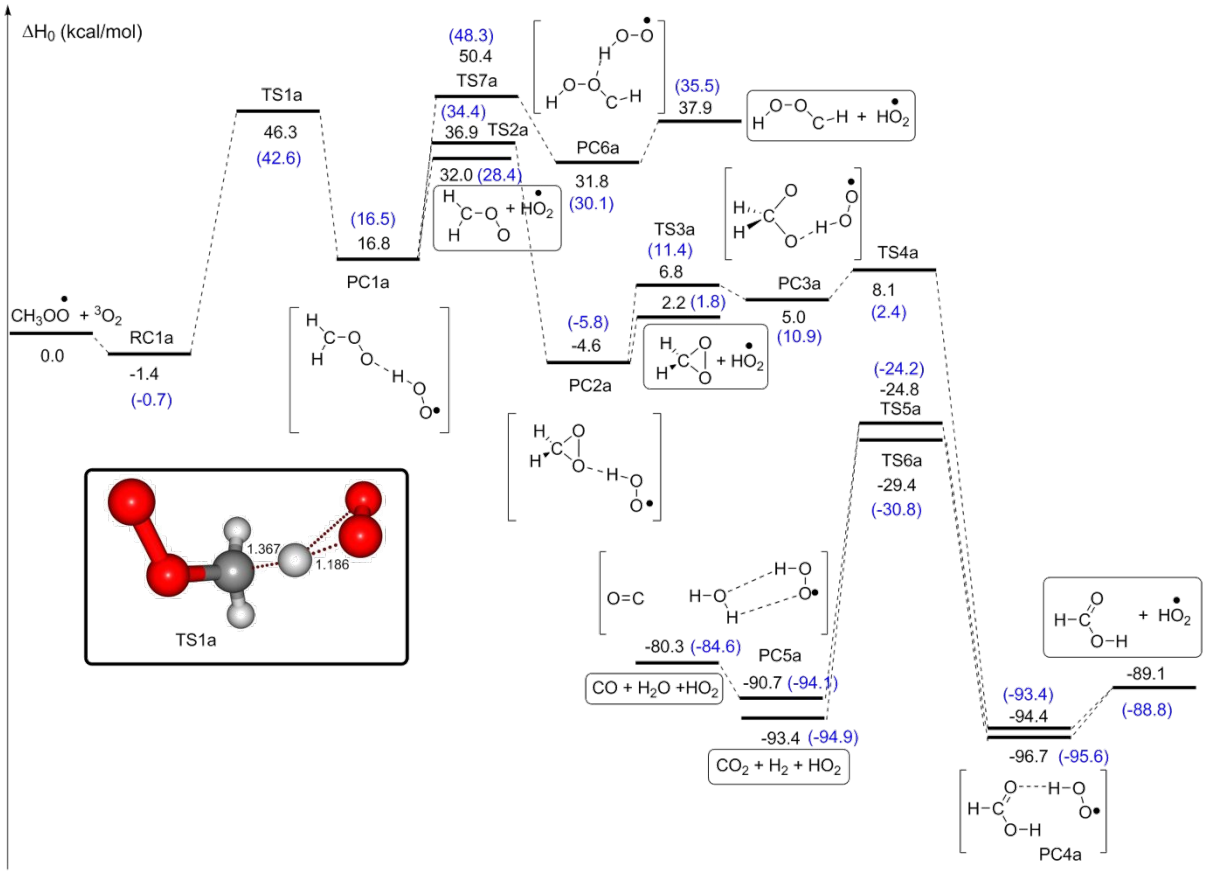


**Figure 1:** PES for the reaction between $CH_3O_2$ and $^3O_2$ through H-atom abstraction calculated at UM06-2X/cc-pVTZ level of theory. The values calculated at UCCSD(T)/cc-pVTZ//UM06-2X/cc-pVTZ level are in parenthesis. Energies, $\Delta H_0(0)$ are in kcal/mol.

The final products of $CH_3O_2$ oxidation through this pathway will be determined mainly from the decomposition routes of highly energetic formic acid product. The PES for formic acid dissociation was studied earlier[30-32] and $CO_2 + H_2$ and $CO + H_2O$ were identified as the main products. PC4a leads to two dissociation pathways, one forming $CO_2 + H_2 + HO_2$ as products and another forming $CO + H_2O + HO_2$ as products. These products are formed through TS5a and TS6a with energy barriers of 71.4 and 64.8 kcal/mol with respect to PC4a. The reactions forming $CO_2 + H_2 + HO_2$ and $CO + H_2O + HO_2$ are highly exothermic by 92.7 and 82.2 kcal/mol, respectively, which is in good agreement with the ATcT[12] values of -94.1 and -84.3 kcal/mol. The $CH_2OO + HO_2$ (PC1a) complex can also undergo H-shift reaction resulting in $HCOOH + HO_2$ through transition state TS7a. The energy barrier required for this H-atom shift reaction is 48.3 kcal/mol, which is 13.9 kcal/mol higher than the energy barrier required for isomerization of $CH_2OO$ to form dioxirane. This shows that the isomerization of $CH_2OO$ is more favourable than the H-atom shift reaction. Thus the main fate of PC1a is its impulsive decomposition into $CH_2OO + HO_2$, which is both entropically

and energetically strongly favored over the reactions via TS2a and TS7a. From the high energy barrier associated with the initial step (TS1a), it may be concluded that the H-atom abstraction pathway is not a likely mechanism for significant $CH_3O_2 + O_2$ reaction.

**$O_2$ addition reaction**

The reaction between $CH_3O_2$ and $O_2$ can also proceed by the addition of $O_2$ to the terminal O-radical site of $CH_3O_2$ and the PES for this reaction is shown in Figure 2. This addition reaction leads to highly oxygenated molecules,[33] a process referred to as extensive autoxidation (EA).[21] The addition reaction takes place on a flat PES with energy barrier of 21.9 kcal/mol and the adduct is 19.1 kcal/mol less stable than the isolated reactants. The energy barrier associated with transition state TS1b of this reaction is 20.7 kcal/mol less than that required for the H-atom abstraction reaction through TS1a. This is because in direct adduct formation transition states, the stabilizing interactions remain mostly intact.[34] The adduct further undergoes an intramolecular H-atom shift of the C-H to the peroxy radical site through TS2b forming an allyl stabilized hydroperoxide radical $CH_2$(OOOOH). In the transition state TS2b, the intramolecular H-transfer reaction is via a five-membered transition state involving the -OO-OOH group. This requires a large energy barrier of 60.2 kcal/mol and the resulting hydroperoxide is 19.5 kcal/mol less stable than the initial adduct. The allyl stabilized hydroperoxide radical then undergoes O-O bond cleavage reaction forming HCHO and $HO_3$ in an exothermic reaction with reaction enthalpy of -18.6 kcal/mol. The O-O bond cleavage occurs through a transition state TS3b with energy barrier of 2.3 kcal/mol with respect to the hydroperoxide and 35.1 kcal/mol with respect to the separated reactant species. The transition states TS2b and TS3b are defined as EA transition states[9] leading to highly oxygenated $HO_3$ species. This very weakly bound species decomposes to OH and $O_2$. The formation of $HO_3$ through $CH_3O_2 + O_2$ reaction gains relevance in combustion chemistry, as a precursor of peroxone which is used to treat petroleum hydrocarbons and diesel fuels.[35] Since the effective energy barrier for reaction by this path, through TS2b, is over 60 kcal/mol, it will not be significant.

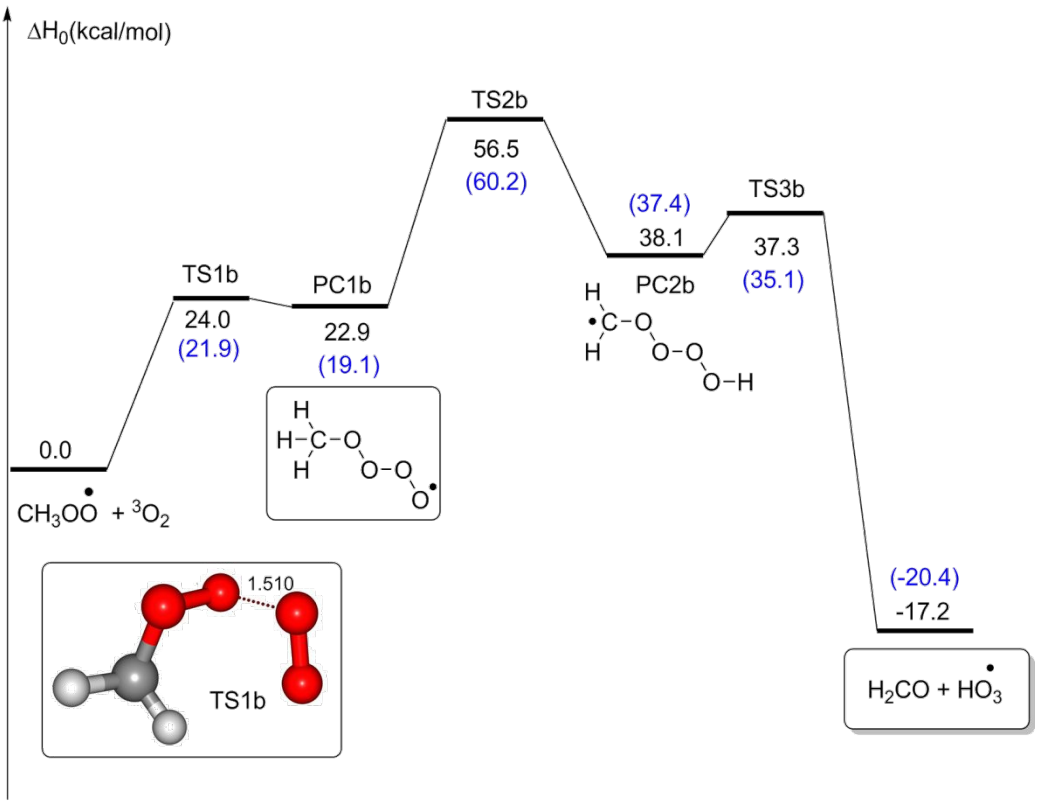


**Figure 2:** PES for the reaction between $CH_3O_2$ and $^3O_2$ through $O_2$ addition calculated at UM06-2X/cc-pVTZ level of theory. The values calculated at UCCSD(T)/cc-pVTZ//UM06-2X/cc-pVTZ level are in parenthesis. Energies, $\Delta H_0(0)$ are in kcal/mol.

**Concerted $O_2$ addition and H-atom shift reaction**

The reaction between $CH_3O_2$ and $O_2$ can also proceed by H-atom shift to the peroxy radical site accompanied by $O_2$-addition to the C-H radical site in a concerted mechanism. The PES for this reaction is presented in Figure 3. Surprisingly, this concerted mechanism is exothermic by -20.6 kcal/mol, revealing that this reaction is the thermodynamically favoured initial step for the reaction between $CH_3O_2$ and $O_2$. The reaction occurs via a tight-transition state TS1c with an energy barrier of 13.5 kcal/mol with respect to the separated reactants. TS1c follows after a pre-reactive complex which lies 3.4 kcal/mol below the reactants adding up the energy barrier to this reaction to be 16.9 kcal/mol. This energy barrier is 5.6 kcal/mol less than TS1b associated with $O_2$ addition reaction.

Because of the odd and difficult-to-locate transition state TS1c, we briefly checked out a few other functionals. All initial attempts to locate TS1c with different functionals and basis sets invariably converged on a transition state structure, TS1c' which eliminated the peroxy group attached to the methyl C and showed the addition of incoming $O_2$ molecule to the C-radical site by simultaneous H-atom abstraction from $CH_3$ group by O-atom. The energy barrier for this process is 51.2 kcal/mol. This is the behaviour which is observed in

dynamic simulations described below, where the post transition state dynamics immediately lead to the elimination of $O_2$ molecule, but it occurs later, not first and at higher energy. The difference between both the transition states is that C-O bond is broken in TS1c' and the degree to which H-atom transferred is major in this transition state, with an elongated C-H bond compared to TS1c. Rather than involving the intermediate PC1c, the new transition state paves the pathway for the direct formation of $H_2CO + OH + O_2$ product channel. This shows that the concerted and the step-wise mechanisms may be mixed and this exploration requires extensive investigation, awaiting future detailed work and benchmarking. In such a situation, where the minimum energy path and the methods employed are inadequate to describe the reaction, dynamic effects are necessary to understand the mechanism. The trajectories obtained through direct dynamics simulations discussed in Section B confirm the existence of the transition state TS1c and the large probability for the reaction of $CH_3O_2 + O_2$ to proceed through TS1c. Therefore, with the results obtained from dynamics simulations we rely on our parameters for now.

The intermediate hydroperoxyalkylperoxy OOQOOH radical formed through TS1c undergoes alpha C-H bond and O-O bond cleavages, forming OH radical along with peroxyformic acid HC(=O)OOH. The transition state TS2c associated with this reaction step is four centered tight transition state involving C-H and O-O bond stretches. TS2c lies 15.9 kcal/mol below the separated reactants and the required energy barrier for HC(=O)OOH + OH complex formation is 4.2 kcal/mol. This reaction is largely exothermic by 100.5 kcal/mol. Unlike the H-atom abstraction reaction which involves formic acid as a key intermediate, the concerted $O_2$ addition and H-atom abstraction reaction involves peroxyformic acid as the key intermediate. The OH radical in the HC(=O)OOH + OH complex further abstracts H-atom from alpha C-H group thereby weakening O-O bond resulting in $CO_2 + H_2O$ and OH products.

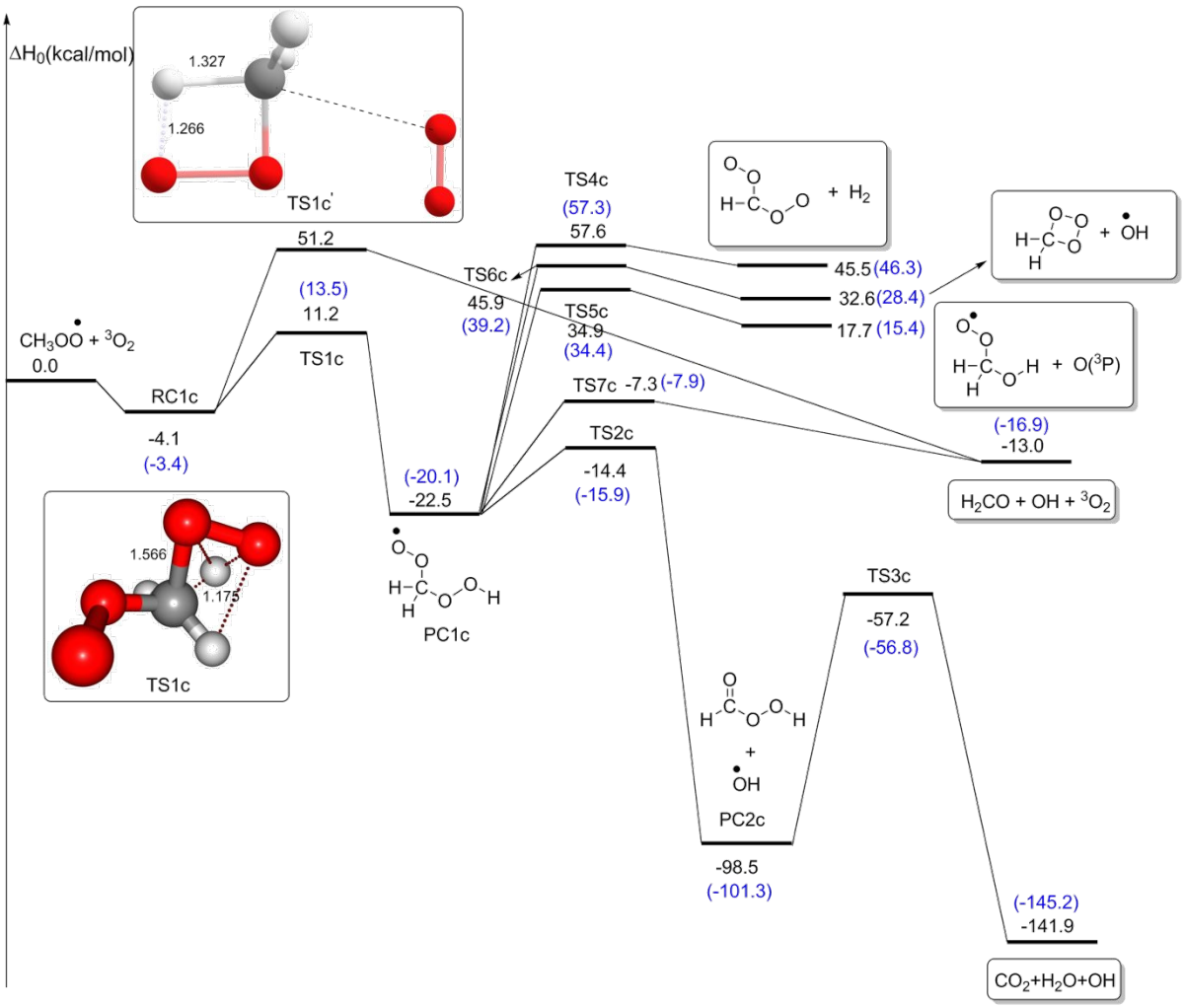


**Figure 3:** PES for the reaction between $CH_3OO$ and $^3O_2$ through concerted $O_2$ addition and H-atom shift calculated at UM06-2X/cc-pVTZ level of theory. The values calculated at UCCSD(T)/cc-pVTZ//UM06-2X/cc-pVTZ level are in parenthesis. Energies, $\Delta H_0(0)$ are in kcal/mol.

The $OOCH_2OOH$ radical can also undergo C-H and O-O bond cleavage forming $H_2$ and an unstable OO(CH)OO radical. The O-O bond cleavage in OOQOOH radical can also result in H-atom shift reaction to the elimination of $O(^3P)$ and formation of $OOCH_2OH$ radical. Another possible reaction from $OOCH_2OOH$ radical is O-O bond cleavage leading to a trioxide and OH radical. Note that all these three reactions take place in a concerted manner in high energy barrier process of 57.3, 34.4, and 39.2 kcal/mol, respectively with reference to $CH_3OO$ + $^3O_2$ reactants via transition states TS4c, TS5c and TS6c. The product channels formed from these reactions are endothermic pathways.

Another interesting reaction from unimolecular dissociation of $OOCH_2OOH$ radical is C-O and O-O bond cleavages in a single kinetic step forming $H_2CO$ + OH + $^3O_2$ in an exothermic reaction with enthalpy of -13.3 kcal/mol. In the associated transition state TS7c,

the C-O bond linking the allyl and the peroxy radical group of $OOCH_2OH$ radical is cleaved, thereby weakening the O-O bond of the hydroperoxide unit. This therefore results in $H_2CO$ + OH + $^3O_2$ products. Since a highly energetic PC1c is formed and the exothermic TS7c is much looser (entropically favoured) than TS2c, these would be the expected products.

**B. Post-transition state dynamics**

Post-transition state dynamics simulations were performed from transition state TS1c in order to determine the most likely products for the concerted channel of the $CH_3O_2$ + $^3O_2$ reaction. The simulations were carried out at 300 K and the corresponding Boltzmann distribution of energy was added to the rotational, vibrational and reaction coordinate degrees of freedom. The trajectories were calculated at UM06-2X/cc-pVDZ level of theory and a total of 100 trajectories were calculated with an integration time step of 2 fs and a total integration time for each trajectory of 2 ps. The probability of products resulting from the post-transition state dynamics of TS1c is shown in Figure 4.

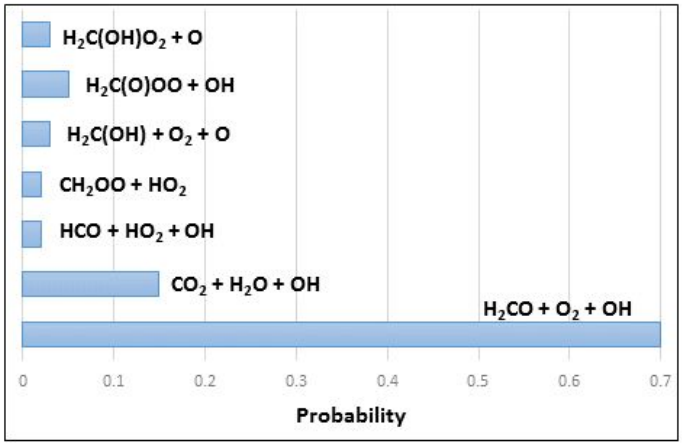


**Figure 4:** Probability of products resulting from TS1c

As shown in Figure 4, the most probable product channel is $H_2CO$ + $O_2$ + OH, followed by $CO_2$ + $H_2O$ + OH, and the least probable channels are $CH_2OO$ + $HO_2$ and HCO + $HO_2$ + OH. Though the products, $CO_2$ + $H_2O$ + OH are formed with a larger exothermicity, its probability is significantly lower (0.15) compared with the $H_2CO$ + $O_2$ + OH product channel (0.70). $H_2CO$ and OH radical are the major products formed, and $CH_2OO$ + $HO_2$ channel is negligible and cannot be an important source of formic acid, which would lead to CO + $H_2O$ and $CO_2$ + $H_2$ product channels. Another minor product channel $H_2C(OH)$ + $O_2$ + O, not calculated in the QM calculations is observed in the dynamic simulations. The

trajectories of these minor product channels if run for a long time beyond 2 ps are expected to lead to $H_2CO$ along with co-products.

A snapshot of the trajectories leading to $H_2CO + O_2 + OH$ products is shown in Figure 5. The reactive events are very rapid such that within 1 ps of time frame the isolated products $H_2CO + O_2 + OH$ are formed. At 0.2 ps, the O-O bond carrying hydroperoxide unit is cleaved and at 0.3 ps, the C-O bond carrying the peroxy radical unit is cleaved. The O-H bond is formed at 0.5 ps and at 0.6 ps, $H_2CO$, $O_2$ and OH are formed with less interactions. The products are almost completely formed at 0.8 ps and finally isolated at 0.9 ps. The products $H_2CO$, $O_2$ and OH remained the same at the end of 2 ps, without undergoing any secondary dissociations. Earlier studies show that the classical barrier for $H_2CO$ dissociation to $H_2 + CO$ is 87.4 kcal/mol[36] and with the transition state ZPE[36] added the energy criterion for dissociation is 98.8 kcal/mol. With this large classical barrier and insufficient internal energy, secondary dissociation of $H_2CO$ is least feasible in the reaction.

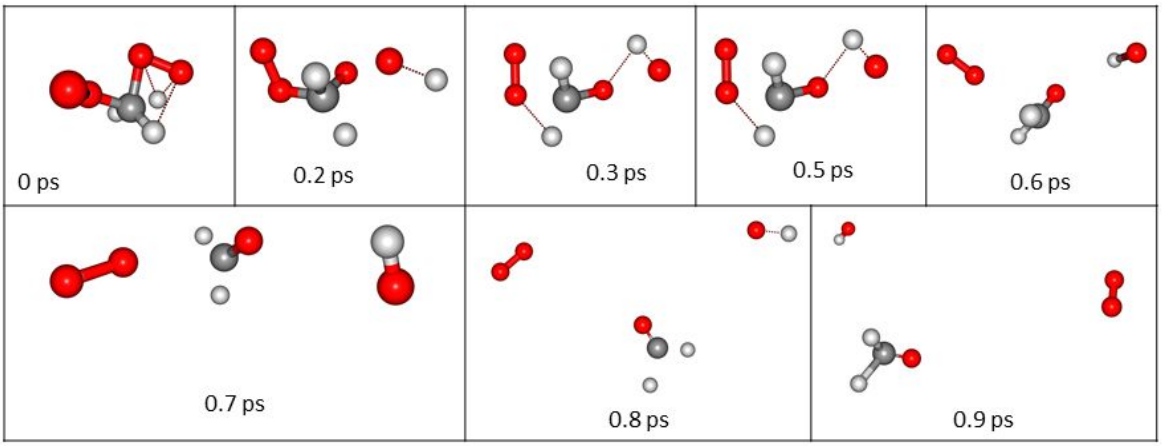


**Figure 5:** Representative snapshots of trajectories for the $H_2CO + O_2 + OH$ product channel.

On comparing the three different initial routes for the $CH_3O_2 + {}^3O_2$ reaction, the concerted H-atom shift and $O_2$ addition pathway is the most favorable reaction both kinetically and thermodynamically. The $O_2$ addition reaction forming a peroxone is the next most likely. In both of these reactions, $H_2CO$ is the major product formed. The traditional H-atom abstraction reaction forming a Criegee intermediate and $HO_2$ is less favored due to a high energy barrier. The dynamics simulations further demonstrate that $CH_2OO$ formed from an H-atom abstraction reaction do not contribute to the formation of the final products from the $CH_3O_2 + O_2$ reaction.

**C. Rate constant values**

Rate constant expressions for modelling use were estimated using theoretical methods from the quantum theory transition state parameters. Transition state theory calculations and stochastic master equation computations were performed with the Multiwell suite of codes.[29]

For the first abstraction channel, we have computed a rate constant expression using simple transition state theory with an energy barrier of 42.6 kcal/mol and the calculated TS1a frequencies given in Table 2. This reasonably assumes no back reaction or effect of the very small RC1a entrance complex. The resulting three parameter rate expression is $467.T^{2.9}e^{-20870/T}$ $cm^3mole^{-1}s^{-1}$. In 1 atm air at 1000K, this would give a $CH_3O_2$ loss rate of only 0.01 $s^{-1}$. The high barrier prevents significant reaction.

Since the second pathway, Figure 2, involves both a high energy barrier and a tight rearrangement transition state TS1b, entropically disfavoured, the rate of this reaction will be very slow. A simple transition state theory calculation yields a rate constant expression of $4.5x10^9e^{-31000/T}$ $cm^3mole^{-1}s^{-1}$ for the reaction $CH_3O_2 + O_2 \rightarrow H_2CO + O_2 + OH$.

The setup for estimating a rate constant for the pathway of Figure 3 consists of 4 steps: formation of the collision complex RC1c with 3.4 kcal/mol stability at a gas kinetic rate, its fast dissociation back to reactants, or reaction via TS1c over a 16.9 kcal/mol barrier, followed by the assumed total decomposition of the resulting $OOCH_2OOH$ PC1c intermediate via the loose TS7c (favoured both by enthalpy and entropy). Only a small fraction of the RC1c will go on to reaction. We performed master equation calculations on the system involving RC1c formation, decomposition to reactants and to products via TS1c. We assumed a rate constant for RC1c formation equal to half the high pressure limit for $CH_3 + O_2 \rightarrow CH_3O_2$, and compute the equilibrium reverse rate for decomposition of RC1c to reactants. The decomposition to products is determined from the TS1c parameters. The Multiwell master equation code[29] was used with the Inverse Laplace Transform (ILT) option for the calculations. No RC1c formation is predicted up to 100 atm above 500 K, and results are pressure independent. A fit of the results yields the expression $4.2x10^{13}e^{-8676/T}$ $cm^3mole^{-1}s^{-1}$. While this is a slow rate, it could still be significant for large oxygen densities. The lifetime of $CH_3O_2$ to this reaction at 1000 K and 1 atm of air would be just 50 μs. This reaction is not chain branching but does transform a less reactive peroxy radical to a more reactive OH and produces a formaldehyde fuel. It may be important for methane combustion in the 1000-

1300K temperature range at high oxygen concentration. At lower temperatures it is too slow and at higher temperatures equilibrium $CH_3O_2$ concentrations are too low.

If one assumes for a high oxygen environment that equilibrium exists between the reactants and the weakly bound RC1c complex, the rate constant can be computed by simple transition state theory involving TS1c. Resulting rate constants are nearly identical to the master equation results ($4840.T^{3.0}e^{-6640/T}$ $cm^3mole^{-1}s^{-1}$), (We also get a similar result from directly computing the steady state RC1c concentration and its TST dissociation rate constant.) This then implies the master equation results are not dependent on the assumed RC1a rate constant, or the accuracy of the shallow RC1c well depth.

**Table 2.** Rate constant calculation parameters

| Transition state | TS1a | TS2b | TS1c |
|---|---|---|---|
| Frequencies (cm-1) | 31.1, 101.6, 115.4, 272.8, 532.4, 564.8, 633.9, 1062, 1085, 1149, 1219, 1325, 1437, 1455, 1513, 3100, 3240 | 152.7, 392.6, 509.2,563.4, 634.2, 738.5,837.3, 916, 1039,1095, 1152, 1219, 1281,1448, 1715, 3078, 3217 | 32.3, 47.0, 65.5, 82.1, 117.9, 282.7, 776, 894, 1018, 1073, 1162, 1167, 1456, 1776, 2033, 3092, 3218 |

## IV. Conclusions

Quantum mechanics computations were undertaken to define the potential energy surface features for the previously unexplored reaction of $CH_3O_2$ with $^3O_2$, in order to assess its possible importance in the lower temperature ignition of methane fuels at high pressure and oxygen concentration. Stationary points identified as intermediates, transition states, and products were computed at the UCCSD(T)/cc-pVTZ//UM06-2X/cc-pVTZ level of theory. Three potential reaction paths were found.

The anticipated H abstraction channel transition state has a high barrier of 42.6 kcal/mol. The products can form a H-bonded complex, capable of undergoing further rearrangements, with likely final products $HO_2 + CO_2 + H_2$ or $HO_2 + CO + H_2O$ from HCOOH decomposition. The direct route from the transition state to $HO_2 + CH_2OO$, is with subsequent rapid decomposition of the Criegee intermediate to $CO + H_2O$. A transition state theory calculation based on the calculated parameters for TS1a gives a rate constant expression for $CH_3O_2 + {}^3O_2 \rightarrow HO_2 + CO + H_2O$ of $467.T^{2.9}e^{-20870/T}$ $cm^3mole^{-1}s^{-1}$.

A second reaction pathway is initiated by $^3O_2$ addition to the peroxy end of $CH_3O_2$, followed by an H atom shift involving an even higher barrier. The second intermediate $CH_2OOOOH$ would decompose to OH + $O_2$ + $H_2CO$ products. This channel has a very low reaction probability.

The third pathway discovered involves a concerted $^3O_2$ addition to the carbon atom of $CH_3O_2$ with H migration to the added O. This follows formation of a weakly bound complex. While further rearrangements to various products can occur, rapid dissociation of the resulting $OOCH_2OOH$ intermediate (PC1c) to $H_2CO$ + OH + $O_2$ is preferred. This was confirmed by trajectory studies. Assuming a rapid formation rate for the complex RC1c, rapid decomposition of the PC1c intermediate, and the computed parameters for TS1c, a transition state theory/master equation calculation estimate gives a rate constant expression for this channel for $CH_3O_2 + {}^3O_2 \rightarrow H_2CO + OH + O_2$ of $4.2x10^{13}e^{-8676/T}$ $cm^3mole^{-1}s^{-1}$. The rate constants will be included in version 2 of the optimized Foundational Fuel Chemistry Mechanism.

**Acknowledgements**

The research reported here is based on work supported by the U.S. Air Force Office of Scientific Research (AFOSR) under Grant No. FA9550-17-1-0119 and the Robert A. Welch Foundation under Grant No. D-0005. The simulations were performed on the Quanah computer cluster of the High Performance Computing Center (HPCC) of Texas Tech University and the Chemdynm computer cluster of the Hase Research Group. Dr. K. Senthilkumar, Bharathiar University is acknowledged for providing computational facilities for performing electronic structure calculations.

**Supplementary material**. Cartesian coordinates of the structures of RC, PC and TS calculated at UM06-2X/cc-pVTZ level, vibrational frequencies calculated at the same level of theory and thermochemistry of the reactions and stationary points studied.

**References:**

(1) Zhu, R.; Hsu, C. C.; Lin, M. C. Ab Initio Study of the $CH_3 + O_2$ Reaction: Kinetics, Mechanism and Product Branching Probabilities. *J. Chem. Phys.* **2001**, *115*, 195−203.
(2) Cobos, C. J.; Hippler, H.; Luther, K.; Ravishankara, A. R.; Troe, J. High-Pressure Falloff Curves and Specific Rate Constants for the Reaction $CH_3 + O_2 \rightarrow CH_3O_2 \rightarrow CH_3O + O$. *J. Phys. Chem.* **1985**, *89*, 4332-4338.
(3) Pilling, M. J.; Smith, C. A Laser Flash Photolysis Study of the Reaction $CH_3 + O_2 \rightarrow CH_3O_2$ at 298 K. *J. Phys. Chem.* **1985**, *89*, 4713-4720.
(4) Kaiser, E. W. Pressure Dependence of the Rate Constants for the Reactions Methyl + Oxygen and Methyl + Nitric Oxide from 3 to 104 Torr. *J. Phys. Chem.* **1993**, *97*, 11681-11688.
(5) Cheung, Y. S.; Li, W. K. An Ab-Initio Molecular-Orbital Study of the $CH_3O_2$ and $CH_3O_2$ + Potential-Energy Surfaces. *J. Mol. Struct.: THEOCHEM* **1995**, *333*, 135−145.
(6) Higgin, R. M. R.; Williams, A. A Shock-Tube Investigation of the Ignition of Lean Methane and n-Butane Mixtures with Oxygen. *J. Symp. Int. Combust. Proc.* **1969**, *12*, 579-590.
(7) Hsu, D. S. Y.; Shaub, W. M.; Creamer, T.; Gutman, D.; Lin, M. C. Kinetic Modeling of CO Production from the Reaction of $CH_3$ with $O_2$ in Shock Waves. *Ber. Bunsen- Ges. Phys. Chem.* **1983**, *87*, 909-919.
(8) Petersen, E. L.; Kalitan, D. M.; Simmons, S.; Bourque, G.; Curran, H. J.; Simmie, J. M. Methane/Propane Oxidation at High Pressures: Experimental and Detailed Chemical Kinetic Modelling. *Proc. Combust. Inst.* **2007**, *31*, 447–454.
(9) Wang,Z.; Popolan-Vaida, D. M.; Chena, B.; Moshammer, K.; Mohamed, S. Y.; Wang, H.; Sioud, S.; Raji, M. A.; Kohse-Höinghaus, K.; Hansen, N.; Dagaut, P; Leone, S. R.; Sarathy, S. M. Unraveling the Structure and Chemical Mechanisms of Highly Oxygenated Intermediates in Oxidation of Organic Compounds. *Proc. Nat. Acad. Sci.* **2017**, *114*, 13102-13107.
(10) Pollard, R. T. *Hydrocarbons. Comprehensive Chemical Kinetics: Gas-Phase Combustion, eds Bamford CH, Tipper CFH (Elsevier, Amsterdam),* **1977**, *17*, 249–368.
(11) Warnatz, J.; Maas, U.; Dibble, R. W. Low Temperature Oxidation, Engine Knock. Combustion: Physical and Chemical Fundamentals, Modeling and Simulation, Experiments, Pollutant Formation (Springer, Berlin), **1999**, 227–236.
(12) Ruscic, B. Active Thermochemical Tables. (Updated Active Thermochemical Tables) (AtcT) Values Based on Version 1.122 of the Thermochemical Network, **2013,** https://atct.anl.gov/Thermochemical%20Data/version%201.122/index.php
(13) Zhao, Y.; Truhlar, D. G. The M06 Suite of Density Functionals for Main Group Thermochemistry, Thermochemical Kinetics, Noncovalent Interactions, Excited States, and Transition Elements: Two New Functionals and Systematic Testing of Four M06-class Functionals and 12 other Functionals, *Theor. Chem. Acc.* **2008**, *120*, 215–241.
(14) Dunning Jr., T. H. Gaussian Basis Sets for Use in Correlated Molecular Calculations. I. The Atoms Boron through Neon and Hydrogen. *J. Chem. Phys.* **1989**, *90*, 1007–1023.
(15) Purvis III, G. D.; Bartlett, R. J. A Full Coupled-Cluster Singles and Doubles Model – the Inclusion of Disconnected Triples. *J. Chem. Phys.* **1982**, *76*, 1910-1918.

(16) Pople, J. A.; Head-Gordon, M.; Raghavachari, K. Quadratic Configuration Interaction – a General Technique for Determining Electron Correlation Energies. *J. Chem. Phys.* **1987**, *87*, 5968-5975.
(17) Montgomery, A.; Frisch, M. J.; Ochterski, J. W.; Petersson, G. A. A Complete Basis Set Model Chemistry. VI. Use of Density Functional Geometries and Frequencies. *J. Chem. Phys.* **1999**, *110*, 2822-2827.
(18) Cord, M.; Sirjean, B.; Fournet, R.; Tomlin, A.; Ruiz-Lopez, M.; Battin-Lece-lerc, F. Improvement of the Modeling of the Low-Temperature Oxidation of n-Butane: Study of the Primary Reactions. *J. Phys. Chem. A* **2012**, *116*, 6142-6158.
(19) Miyoshi, A. Systematic Computational Study on the Unimolecular Reactions of Alkylperoxy ($RO_2$), Hydroperoxyalkyl (QOOH), and Hydroperoxyalkylperoxy ($O_2QOOH$) Radicals. *J. Phys. Chem. A* **2011**, *115*, 3301-3325.
(20) Frisch, M. J.; Trucks, G. W.; Schlegel, H. B.; Scuseria, G. E.; Robb, M. A.; Cheeseman, J. R.; Scalmani, G.; Barone, V.; Mennucci, B.; Petersson, G. A.; Nakatsuji, H.; Caricato, M.; Li, X.; Hratchian, H. P.; Izmaylov, A. F.; Bloino, J.; Zheng, G.; Sonnenberg, J. L.; Hada, M.; Ehara, M.; Toyota, K.; Fukuda, R.; Hasegawa, J.; Ishida, M.; Nakajima, T.; Honda, Y.; Kitao, O.; Nakai, H.; Vreven, T.; MontgomeryJr. J. A.; Peralta, J. E.; Ogliaro, F.; Bearpark, M.; Heyd, J. J.; Brothers, E.; Kudin, K. N.; Staroverov, V. N.; Kobayashi, R.; Normand, J.; Raghavachari, K.; Rendell, A.; Burant, J. C.; Iyengar, S. S.; Tomasi, J.; Cossi, M.; Rega, N.; Millam, J. M.; Klene, M.; Knox, J. E.; Cross, J. B.; Bakken, V.; Adamo, C.; Jaramillo, J.; Gomperts, R.; Stratmann, R. E.; Yazyev, O.; Austin, A. J.; Cammi, R.; Pomelli, C.; Ochterski, J. W.; Martin, R. L.; Morokuma, K.; Zakrzewski, V. G.; Voth, G. A.; Salvador, P.; Dannenberg, J. J.; Dapprich, S.; Daniels, A. D.; Farkas, Ö.; Foresman, J. B.; Ortiz, J. V.; Cioslowski, J.; Fox, D. J. *Gaussian 09*, Revision D.01, Gaussian, Inc., Wallingford CT, 2009.
(21) Hase, W. L.; Duchovic, R. J.; Hu, X.; Komornicki, A.; Lim, K. F.; Lu, D. H.; Peslherbe, G. H.; Swamy, S. R.; Vande Linde, S. R., Varandas, A.; Wang, H.; Wolf, R. J. Quantum Chem. Program Exch. *(QCPE) Bull*. **1996**, *16*, 43.
(22) Hu, X.; Hase, W. L.; Pirraglia, T. Vectorization of the General Monte Carlo Classical Trajectory Program VENUS. *J. Comp. Chem.* **1991**, *12*, 1014-1024.
(23) Lourderaj, U.; Sun, R.; Kohale, S. C.; Barnes, G. L.; de Jong, W. A.; Windus, T. L.; Hase, W. L. The VENUS/NWChem Software Package. Tight Coupling between Chemical Dynamics Simulations and Electronic Structure Theory. *Comput. Phys. Commun*. **2014**, *185*, 1074-1080.
(24) Peslherbe, G. H.; Wang, H.; Hase, W. L. Monte Carlo Sampling for Classical Trajectory Simulations. *Adv. Chem. Phys.* **1999**, *105*, 171-201.
(25) Schlier, C.; Seiter, A. Symplectic Integration of Classical Trajectories: A Case Study *J. Phys. Chem. A* **1998**, *102*, 9399-9404.
(26) Schlier, C.; Seiter, A. High-Order Symplectic Integration: An Assessment. *Comput. Phys. Commun*. **2000**, *130*, 176-189.
(27) Sun, L.; Park, K.; Song, K.; Setser, D. W.; Hase, W. L. Use of a Single Trajectory to Study Product Energy Partitioning in Unimolecular Dissociation: Mass Effects for Halogenated Alkanes. J. Chem. Phys. 2006, 124, 064313.

(28) Pratihar, S.; Ma, X.; Xie, J.; Scott, R.; Gao, E.; Ruscic, B.; Aquino, A. J. A.; Setser, D. W.; Hase, W. L. Post-transition State Dynamics and Product Energy Partitioning following Thermal Excitation of the F· · · $HCH_2CN$ Transition State: Disagreement with Experiment. *J. Chem. Phys.* **2017**, *147*, 144301-14.
(29) Barker, J. R. Energy Transfer in Master Equation Simulations: A New Approach. *Int. J. Chem. Kinetics*, **2009**, *41*, 748-763.
(30) Goddard, J. D.; Yamaguchi, Y.; Schaefer, H. F. The Decarboxylation and Dehydration Reactions of Monomeric Formic Acid. *J. Chem. Phys.* **1992**, *96*, 1158-1166.
(31) Francisco, J. S. A Comprehensive Theoretical Examination of Primary Dissociation Pathways of Formic Acid. *J. Chem. Phys.* **1992**, *96,* 1167-1175.
(32) Lakshmanan, S.; Pratihar, S.; Machado, F. B. C.; Hase, W. L. Direct Dynamics Simulation of the Thermal 3CH2 + 3O2 Reaction. Rate Constant and Product Branching Ratios. *J. Phys. Chem. A* **2018**, *122*, 4808-4818.
(33) Wang, Z.; Zhang, L.; Moshammer, K.; Popolan-Vaida, D. M.; Shankar, V. S. B.; Lucassen, A.; Hemken, C.; Taatjes, C. A.; Leone, S. R.; Kohse-Höinghaus, K.; Hansen, N.; Dagaut, P.; Sarathy, S. M. Additional Chain-Branching Pathways in the Low-temperature Oxidation of Branched Alkanes. *Combust. Flame* **2016**, *164*, 386-396.
(34) Vereecken, L.; Harder, H.; Novelli, A. The Reaction of Criegee intermediates with NO, $RO_2$, and $SO_2$, and their Fate in the Atmosphere. *Phys. Chem. Chem. Phys.* **2012,** *14*, 14682-14695.
(35) Xu, X.; Goddard III, W. A. Peroxone Chemistry: Formation of $H_2O_3$ and Ring-$(HO_2)(HO_3)$ from $O_3/H_2O_2$. *Proc. Nat. Acad. Sci.* **2002**, *99*, 15308-15312.
(36) Shepler, B. C.; Han, Y; Bowman, J. M. Are Roaming and Conventional Saddle Points for $H_2CO$ and $CH_3CHO$ Dissociation to Molecular Products Isolated from Each Other. *J. Phys. Chem. Lett.* **2011**, *2*, 834 - 838.